VOL. 17, NO. 9, MAY 2022 ISSN 1819-6608
ARPN Journal of Engineering and Applied Sciences

www.arpnjournals.com

STRUCTURAL AND MAGNETIC PROPERTIES OF NICKEL DOPED Fe_3O_4 NANOPARTICLES FOR WASTEWATER REMEDIATION

Erwin Amiruddin[1], Salomo Sinuraya[1], Amir Awaluddin[2], Roulina Sidabutar[3], Syahrizan[3] and Dwi Lutfi Handayani[3]
[1]Department of Physics, Faculty of Mathematics and Natural Sciences, Riau University, Pekanbaru, Indonesia
[2]Department of Chemistry, Faculty of Mathematics and Natural Sciences, Riau University, Pekanbaru, Indonesia
[3]Magnetic Laboratory, Faculty of Mathematics and Natural Sciences, Riau University, Indonesia
E-Mail: erwin_amiruddin@yahoo.com

ABSTRACT

Nickel doped Fe_3O_4 nanoparticles were prepared using ball milling method by varying the different wt.% of nickel. The influence of nickel content on physical properties including structural, magnetic, morphological properties and elemental content of Fe_3O_4 nanopareticles were studied using X-ray diffraction (XRD), vibrating sample magnetometer (VSM), scanning electron microscopy (SEM) and X-ray fluorescence (XRF) spectroscopy, respectively. XRD patterns of prepared samples were indexed to cubic structure and confirmed that undoped sample consists only Fe_3O_4 (magnetite) phase, while the nickel doped samples show two phases including Fe_3O_4 and nickel phase. Moreover, XRD peaks of nickel doped samples shift to slightly lower angles as compared to that of undoped sample resulting increase of crystallite size (29 to 32 nm). These results together with SEM measurements show that the size of the nanoparticles increases with increasing nickel content. Magnetic studies indicated that, in comparison to undoped sample, the saturation magnetization (Ms) of nickel doped samples increases with increasing nickel content. Comparison of elemental composition from raw material to undoped and nickel doped samples shows that the Fe and Ti content increase after being milled, while some impurities such as Al, Si, Ca and others decrease. Hence, based on the observed values of physical properties of the nickel doped Fe_3O_4 nanoparticles makes them applicable as an efficient material for wastewater remediation.

Keywords: Fe_3O_4 nanoparticles, nickel doped, ball milling, Ulakan and physical properties.

INTRODUCTION

In recent years, iron oxides such as α-Fe_2O_3 and γ-Fe_2O_3 and Fe_3O_4 in nanometer scale have special importance due to their potential use in fields ranging from magnetic data storage [1] to biomedical [2] and environmental applications [3]. Among these iron oxide phases for wastewater remediation, Fe_3O_4 nanoparticles are most considerably use due to their notable improvement in properties such as magnetic [4] and catalysis [5]. It is known that Fe_3O_4 can be extracted from natural sand [6]. Commonly, Fe_3O_4 nanoparticles has cubic structure and called magnetite. In order to obtain the desired magnetic and catalytic properties, physical parameters such as crystallite size, morphology, and composition of the samples have to be controlled to make them applicable to a wide range of fields. It is well known that the distinctive magnetic properties of Fe_3O_4 nanoparticles due to the electron transfer between Fe^{2+} and Fe^{3+} ions in the octahedral sites. Several strategies have been developed to improve the magnetic and catalytic properties of Fe_3O_4 nanoparticles. One of them is by introducing the transition elements, such as Al, Mn, Zn and Cu [7, 8, 9] into the structure of Fe_3O_4. For example Varshney, 2011 [8] reported that saturation magnetization of Fe_3O_4 nanoparticles was found to be either decreased or increased depends on nature of the metals and particle size.

To improve the structural, magnetic, morphological properties and compositional of undoped and nickel doped Fe_3O_4 nanoparticles, we here report preparation and physical properties of undoped and nickel doped Fe_3O_4 nanoparticles using ball milling method. Nickel content was varied in the range 0 wt.% - 15 wt.%. Structural and magnetic and morphological properties as well as elemental composition of the samples are correlated with variation in nickel content.

EXPERIMENTAL PROCEDURE

Raw Material and Chemical

Raw material used for preparing Fe_3O_4 nanoparticles is sand beach of Ulakan-Pariaman-West Sumatera. The chemical used for doping the Fe_3O_4 nanoparticles is nickel with purity of 99.99%.

Preparation of Undoped and Nickel Doped Fe_3O_4 Nanoparticles

Fe_3O_4 nanoparticles were prepared using ball milling method using beach sand of Ulakan-Pariaman-West Sumatera as raw material. The sand beach was dried prior to iron sand separator (ISS) process. The product of ISS was milled for 120 h with milling ball size of 1.5 cm. The ball milling product was divided into 4 parts, the first, second, third and fourth part was each doped with nickel with content of 0, 5 and 10 wt.%.

Characterization

The physical properties of undoped and nickel doped Fe_3O_4 nanoparticles were studied by the following techniques: X-ray diffraction (XRD) vibration sample magnetometer (VSM), Scanning Electron Microscopy (SEM) and X-Ray Fluorescence (XRF) spectroscopy.

RESULTS AND DISCUSSIONS

Structural Properties

The X-Ray diffraction patterns of undoped and nickel doped Fe_3O_4 nanoparticles were determined using X-Ray Diffractometer. The x-ray diffraction (XRD) patterns of the samples are dominated with narrow sharp and high diffraction peaks confirming the crystallinity of prepared nanoparticles as shown in Figure-1. The XRD pattern of undoped Fe_3O_4 nanoparticles shows diffraction peaks at 2θ 30.39°, 35.42°, 37.06°, 43.03°, 53.45°, 56.92° and 62.44° which correspond to hkl planes of (200), (311), (222), (400), (422), (511) and (440) Fe_3O_4, respectively [18]. All observed diffraction peaks matched well with the reported JCPDS No. 03-0863 data and can be indexed to cubic structure with lattice parameters of 8.393 Å [19].

The interplanar spacing (d_{hkl}) between the diffraction planes and average crystallite size of undoped and nickel doped Fe_3O_4 nanoparticles are calculated using the well known Bragg [20] and Scherrer [21] shown in Eq. 1 and 2 respectively and the results are summarized in Table-1.

$$2d_{hkl} \sin\theta = n\lambda \quad \text{..... (1)}$$

$$D = \frac{K\lambda}{\beta \cos\theta} \quad \text{..... (2)}$$

where n is an integer called order of reflection, D is the crystallite size (nm), λ is the X-ray wavelength (λ= 1.5406 Å), k is the Scherrer constant, which equals 0.9, β is the full width at half maximum (FWHM) of peaks and θ is the corresponding diffraction angle (degree). In general, the mean crystallite sizes increase with increasing amount of nickel content in the samples. Some researchers [22] use the diffraction peak (311) in order to estimate the values of crystallite size (D). The XRD pattern reveals that (311) peak shifts towards lower angle with increasing content of nickel. This shifting of diffraction peaks result in the increase of crystallite size as shown in Table-1. These results together with SEM measurements show that the size of the nanoparticles increase with increasing nickel content as shown in SEM photographs Figure-3 (b) and (c).

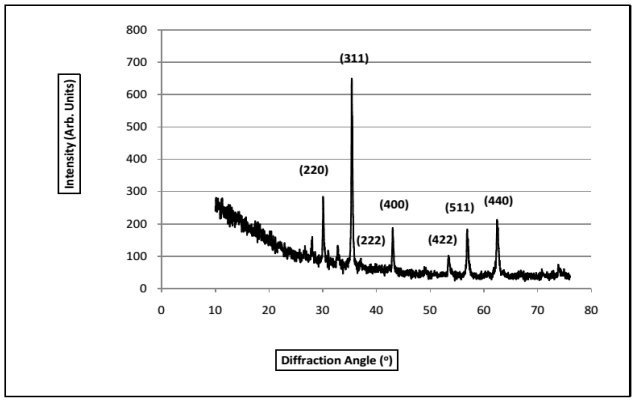

(a)

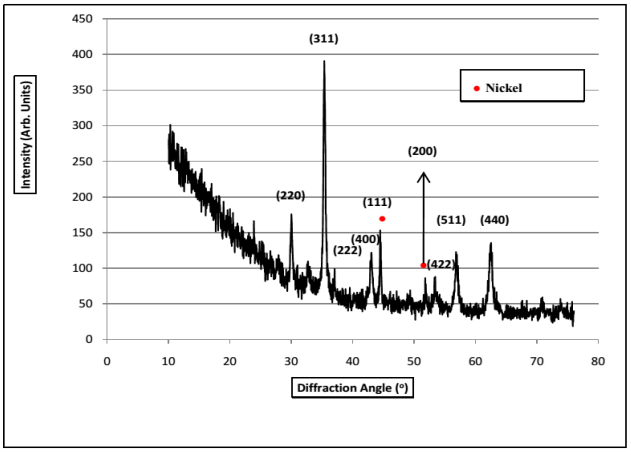

(b)

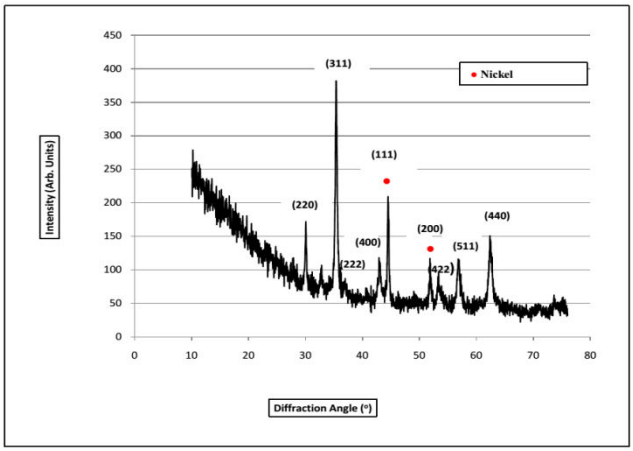

(c)

Figure-1. X-Ray Diffraction patterns of (a) undoped (b) 5 wt.% nickel doped and (c) 10.wt.% nickel doped Fe_3O_4 nanoparticles.

The XRD pattern at 5 wt.% and 10 wt.% of nickel doped magnetite nanoparticles shown in Figure-1(b) and (c) also indicates the formation of cubic structure which reveals the Miller indices such as (220) (311) (222) (400) (422) (511) (214) and (440), these values are agree with the JCPDS No. 03-0863 data. The average crystalline size is calculated based on Scherrer formula (1) for the 5 wt.% and 10 wt.% nickel doped Fe_3O_4 sample as 31.61 and 32.09 nm, respectively. In the XRD patterns of nickel doped Fe_3O_4 Figure-1(b) and (c) two additional diffraction peaks, one at 2θ= 44.5° and other at 2θ= 51.8°, can be seen clearly. These two low intensity diffraction peaks indicated the presence of metallic nickel nanoparticles in the sample. Hence, the existence of diffraction peaks related to the nickel and Fe_3O_4 nanoparticles, showed successful formation of Fe_3O_4-nickel composite using ball milling method. Moreover, the obvious reduction of the intensity of (311) peak with increasing nickel concentration (wt.%) is significant. Note that the peak (222) of Fe_3O_4 nanoparticles is obviously decreased in 10 wt.% nickel doped samples confirmed the increase of crystallite size. Furthermore, the intensity of the nickel diffraction peaks increases when nickel content

increases from 5 wt.% to 10 wt.% which are indexed to (111) and (200) hkl planes of nickel face centered cubic unit cell. This indicates that dominant presence of nickel phase of the samples.

Table-1. Structural parameters of undoped and nickel doped Fe_3O_4 nanoparticles.

Nickel Content (wt.%)	2θ (degree)	Intensity (Arb. Units)	d_{hkl} (Å)	Crystallite Size (nm)
0	35.4151	633.8963	2.5344	29.63
5	35.3631	391.2304	2.5362	31.61
10	35.3371	361.4081	2.5381	32.09

Table-2 shows comparison of elemental composition from Ulakan beach sand to undoped and nickel Fe_3O_4 nanoparticles identified using by x-ray fluorescence (XRF). It is clear that the Fe and Ti concentration increase after ball milling process, while some impurities such as Al, Si, Ca, and others decrease. Therefore, the ball milling process is able to purify the magnetic element and reduce the other elements. It is shown that the nickel composition increase after being doped with nickel (10 wt.%). On the other side, Fe composition decreases and some impurities such as Al, Si, Ca, Ti and others were also decreased.

Table-2. Comparison of elemental composition from Ulakan beach sand to undoped and nickel Fe_3O_4 nanoparticles.

Compound	Concentration (%)		
	Natural Sand	Undoped Fe_3O_4 Nanoparticles	10 wt.%-Nickel Doped Fe_3O_4 Nanoparticles
Al	14.425	1.928	1.436
Si	59.224	7.59	5.523
Ca	10.047	1.921	1.618
Ti	0.926	8.791	7.754
Fe	8.224	75.211	65.696
Ni	0.001	0.014	14.048
Others	7.153	4.545	3.925
Total	100	100	100

Magnetic Properties

Magnetic properties of the samples were investigated using a vibrating sample magnetometer (VSM) with an applied magnetic field of -20000 Oe to +20000 Oe. Figure-2 shows the hysteresis loop of the samples. It is clearly noticed that the hysteresis loops of all samples show ferromagnetic behavior characterized by high coercivity (278.76 - 532.36 Oe). The saturation magnetization (Ms) of the undoped Fe_3O_4 nanoparticles is about 28.23 emu/g. This value is lower that of pure Fe_3O_4 phase (92 emu/g) [23]. The lower value of saturation magnetization values of the samples may be caused by the presence of other metal oxide as indicates in XRF result in Table-2. It is well known that magnetization of ferromagnetic materials is affected by the crystal structure and morphology of prepared samples. The saturation magnetization values of nickel doped samples increase from 28.23 - 31.42 emu/g with increasing nickel content 0 - 10 wt.%, respectively as shown in Table-3. The increase in saturation magnetization observed for the samples prepared with nickel doped could be due to the effect of increased number of magnetic moment to volume ratio associated with particle size [24]. Although nickel has a high magnetic moment, the resulting undoped and nickel doped Fe_3O_4 nanoparticles have a relatively low saturation magnetization compared to that of pure Fe_3O_4 phase. This believes that the magnetic moments in the samples do not have parallel alignment but rather have random orientation.

Remanent magnetization values (Mr) of undoped Fe_3O_4 nanoparticles increases rapidly as nickel content increases to 5 wt.% as shown in Table-3. However, a slowly decrease in Mr values was observed by further increasing nickel content to 10 wt.%, which might be because of the presence of more nickel at the grain boundaries as seen in the XRD results Figure-1(b) and (c) with a slight increase in crystallite size. The coercivity of the Fe_3O_4 nanoparticles increases rapidly when increasing nickel content up to 5 wt. %, and slowly decreases upon further increase in nickel content. The initial increase in coercivity value is due to the contribution of surface anisotropy [25]. It is believe that Fe−Nickel interactions are responsible for the increase in magnetic anisotropy while Nickel-nickel interactions at high nickel content reduce the anisotropy consequently slowly reduces the coercivity values [26].

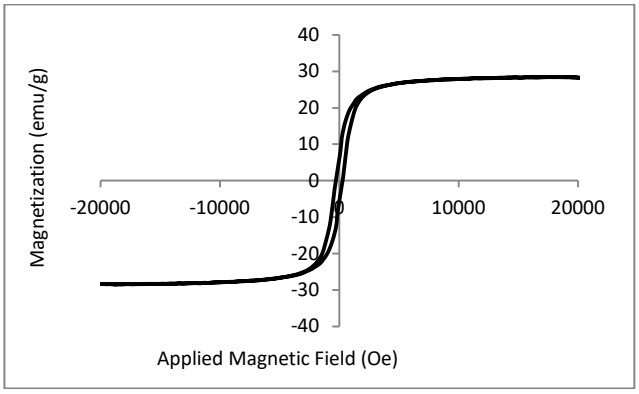

(a)

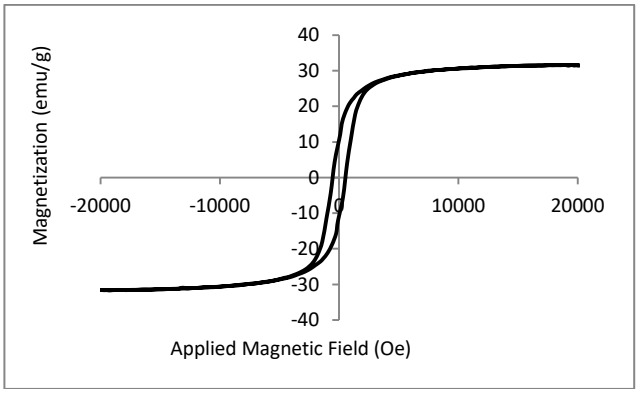

(b)

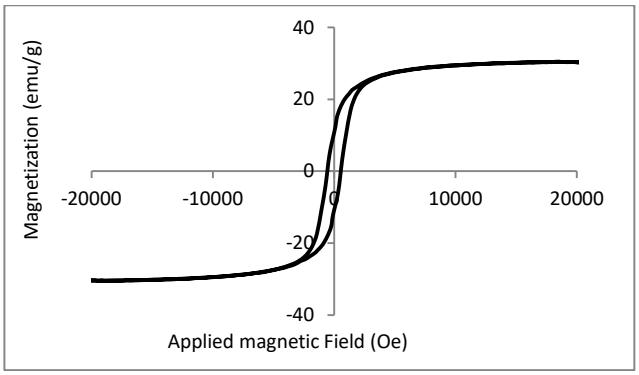

(c)

Figure-2. Hysteresis loops of Fe_3O_4 nanoparticles (a) un doped and nickel doped (b) 5 wt.% and (c) 10 wt.%.

Table-3. Loop hysteresis parameters for undoped and nickel doped Fe_3O_4 nanoparticles.

Nickel Content (wt.%)	Ms (emu/g)	Mr (emu/g)	Hc (Oe)	Loop Squareness (Mr/Ms)
0	28.23	5.82	278.76	5.82
5	30.31	10.57	550.65	10.57
10	31.42	10.43	532.36	10.43

Morphological Properties of Fe_3O_4 Nanoparticles

The morphology of undoped Fe_3O_4 nanoparticles and nickel doped Fe_3O_4 nanoparticles are studied by Scanning electron microscopy (SEM) images with 10.000-x magnification as shown in Figure-3 (a), (b) and (c). From the figure it is clear that, in all the samples, the particles are irregular in shape and randomly organized. The average particle size estimated from these images for undoped Fe_3O_4 is roughly 127 nm. The average particle size increases to 131 nm observed with increasing nickel to 5 wt.%. Further increase in nickel content (10 wt.%), there is a smaller increase in the size of the Fe_3O_4 nanoparticles (137 nm) and these findings are in good agreement with average crystallite size values obtained from XRD measurements. The SEM photograph also shows the agglomerated form of 10 wt.% nickel doped Fe_3O_4 nanoparticles. This is due to the high surface energy possessed by nanoparticles [27]. It shows that the morphology of Ni-doped sample is significantly changed especially for nickel content of 10 wt.% as compared to that for undoped and 5 wt.% nickel doped samples. Therefore, in order to vary the nanoparticle size, the presence of nickel has to be considered [28]

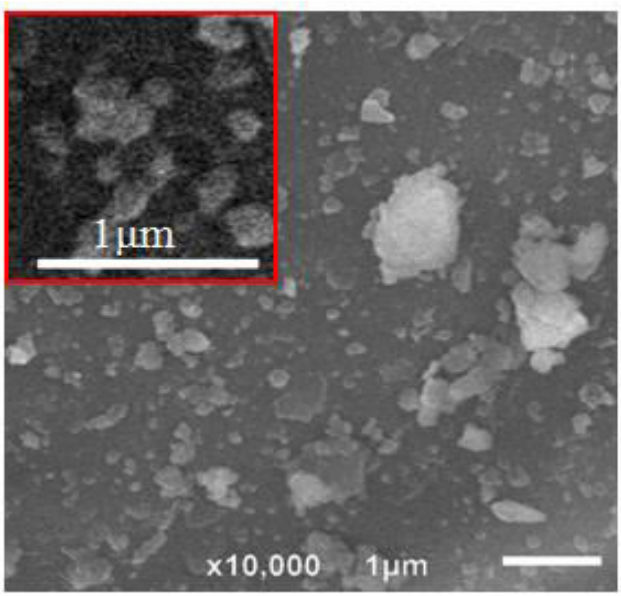

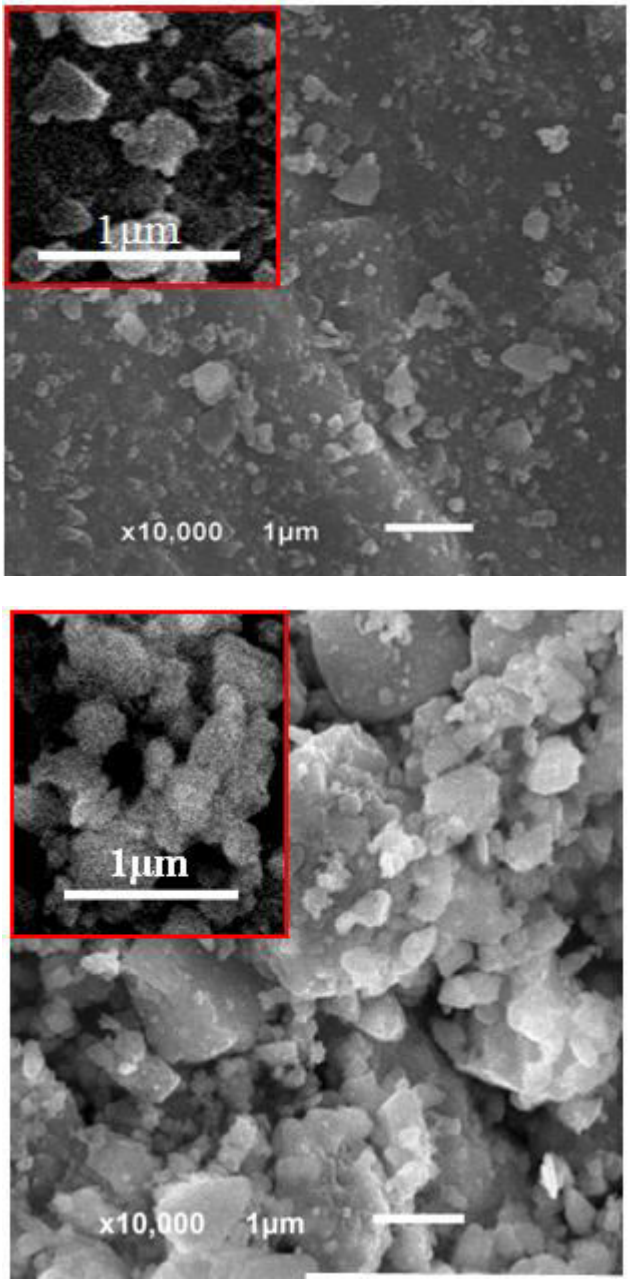

Figure-3. Scanning electron microscopy (SEM) photo graphs for (a) undoped Fe_3O_4 and nickel doped Fe_3O_4 nanoparticles (b) 5 wt.% and (c) 10 wt.%.

CONCLUSIONS

Undoped and nickel doped Fe3O4 nanoparticles have been prepared by ball milling method. The XRF results show that the samples consist of Fe, Ti, Al, Si Ca, Ni and others. The XRD measurement indicates the formation of Fe_3O_4 phase in both undoped and nickel doped Fe_3O_4 nanoparticles. However, two additional diffraction peaks at $2\theta = 44.5°$ and 51.8°, are clearly observed. These two diffraction peaks indicated the presence of metallic nickel nanoparticles in the samples. All diffraction peaks matched well with Fe_3O_4 data and are indexed as cubic structure. The average crystallite size calculated using Scherrer equation increases with increasing nickel content. The results of magnetic measurements show that the samples have a ferromagnetic behavior. Nickel doped Fe_3O_4 nanoparticles were observed to have relatively higher magnetization value compared to that for undoped sample. The SEM image shows that the samples consist of irregular shapes and revealed that the average size of undoped and nickel doped Fe_3O_4 nanoparticles increases with increasing nickel content.

ACKNOWLEDGMENTS

This work was financially supported by the Directorate General of Higher Education, Indonesian Ministry of Education and Culture, 2021. The authors are grateful to Indonesian Sciences Institute (LIPI), for conducting the VSM measurement, Physics department UNP Padang for XRD and XRF measurements, and department of Chemistry ITB Bandung for SEM measurement and to magnetic research member in Magnetism Laboratory FMIPA UNRI, for their assistance during sample collection and preparation.

REFERENCES

[1] Frey N. A., Peng S., Cheng K., Sun S. 2009. Magnetic nanoparticles: Synthesis, functionalization, and applications in bio imaging and magnetic energy storage. Chem. Soc. Rev. 38, pp. 2532-2542.

[2] Colombo M., Carregal-Romero S., Casula M. F., Gutierez L., Morales M. P., Bohm I. B., Heverhagen J. T., Prosperi D., Parak W. J. 2012. Biological applications of magnetic nanoparticles. Chem. Soc. Rev. 41, pp. 4306-4334.

[3] Y. Tuo, G. Liu, B. Dong *et al.* 2015. Microbial synthesis of Pd/Fe_3O_4, Au/Fe_3O_4 and PdAu/Fe_3O_4 nanocomposites for catalytic reduction of nitroaromatic compounds. Scientific Reports. 5(1): 13515-13527.

[4] Jiang M., Peng X. 2017. Anisotropic Fe_3O_4/Mn_3O_4 hybrid nanocrystals with unique Magnetic properties. Nano Lett. 17: 3570-5.

[5] T. Kamakshi and G. Sunitasundari. 2020. Photocatalytic Degradation of Methylene Blue via Cobalt Doped Fe_3O_4 Nanoparticles. Asian Journal of Chemistry. 32(6): 1413-1420.

[6] Erwin Amiruddin, Heri Hadianto, Martha Riana, Salomo Sinuraya, Mohammad Deri Noverdi and Ainun Syarifatul Fitri. 2021. Undoped and manganese doped iron oxide nanoparticles for environmental applications. ARPN Journal of Engineering and Applied Sciences. 16(18): 1872-1876.

[7] Wang X., Hu, C. G., Xi Y., Xia C. H. and He X. S. 2010. Al-doped Fe_3O_4 nanoparticles and their magnetic properties. Journal of Superconductivity and Novel Magnetism. 23: 909-911.

[8] Varshney D., Verma K. and Yogi A. 2011. Structural and magnetic properties of Mn and Zn doped Fe_3O_4 nanoparticles. AIP Conference Proceedings. 1349: 253-254.

[9] Tripathy D., Adeyeye A. O., Boothroyd C. B. and Shannigrahi S. 2008. Microstructure and magneto transport properties of Cu doped Fe_3O_4 films. Journal of Applied Physics. 103: 07F701-07F703.

[10] Amiruddin E., Awaluddin A., Sihombing M., Royka A. and Syahrul T. 2020. Morphology and structural properties of undoped and cobalt doped magnetic iron oxide particles for improving the environmental quality. International Journal of Engineering and Advanced Technology (IJEAT) 2020, 9(6) , pp. 18-21

[11] A. A. Ismail, D. W. Bahnemann, L. Robben, M. Wark. 2010. Palladium doped porous titania photocatalysts: Impact of mesoporous order and crystallinity, Chem. Mater. 22, pp.108-116.

[12] M. H. H. Mahamoud, A. A. Ismail, M. S. S. Sanad. 2012. Developing a cost-effective synthesis of iron oxide doped titania photo catalysts loaded with palladium, platinum or silver nanoparticles, Chem. Eng. J. 187, pp. 96-103.

[13] H. Liang, X. Jiang, W. Chen, S. Wang, B. Xu, Z. Wang. 2014. Ceram. Int. 40: 5653-5658.

[14] Qin D. D., Li Y. L., Wang T., Li Y., Lu X. Q., Gu J., Zhao, Y. X., Song, Y. M., Tao C. L. 2015. Sn Doped Hematite Films as Photoanodes for Efficient Photo electrochemical Water Oxidation, J.Mater. Chem. A 3(13): 6751-5.

[15] Hou J., Cheng H., Yang C., Takeda O. and Zhu H. 2015. Hierarchical carbon quantum dots/hydrogenated-γ-TaON hetero junctions for broad spectrum photo catalytic performance. Nano Energy. 18, 143-153.

[16] Liu Y., Yu Y. X., Zhang W. D. 2012. Photo electrochemical Properties of Ni-Doped Fe_2O_3Thin Films Prepared by Electro deposition. Electrochim. Acta. 59, pp. 121-127.

[17] Dong, W. *et al.* 2016. Preparation of secondary mesopores in mesoporous anatase-silica nanocomposites with unprecedented-high photocatalytic degradation performances. Adv. Funct. Mater. 26, pp. 964-976.

[18] Arularasu M. V., Devakumar J., Rajendran T. V. 2018. An innovative approach for green synthesis of iron oxide nanoparticles: Characterization and its photocatalytic activity. Polyhedron. 156, pp. 279-290.

[19] Ulbrich K., Holá K., Šubr V. *et al*. 2016. Targeted drug delivery with polymers and magnetic nanoparticles: covalent and noncovalent approaches, release control, and clinical studies. Chem. Rev. 116: pp.5338–5431.

[20] Cullity B. D. and Stock S. R. 2001. *Elements of X-Ray Diffraction.* Upper Saddle River, NJ Prentice Hall.

[21] P. Sahay and R. Nath. 2008. Sens. Actuators B, 134, 654. doi:10.1016/j.snb.2008.06.006.

[22] C. L. Huang and E. Maijevic. 1996. Sol. St. Ionics 84, 249.

[23] Can M. M., Ozcan S. C., Ceylan A., Firat T. 2010. Effect of milling time on the synthesis of magnetite nanoparticles by wet milling. Mater Sci Eng B. 172, pp. 72-75.

[24] John R. Reitz and Frederick J. Milford. 1960. *Foundations of Electromagnetic Theory*, Addison Wesley Publishing Company Inc. Reading, Massachusetts, U.S.A. London, England.

[25] E. Lima, A. L. Brandl, A. D. Arelaro and G. F. Goya. 2006. J. Appl. Phys. 99, pp. 83908.

[26] Mørup S., Hansen M. F., Frandsen C. 2010. Magnetic Interactions between Nanoparticles. Beilstein J. Nanotech. 1, pp.182-190.

[27] S. Sagadevana, Z. Z. Chowdhuryb and R. F. Rafiquec. 2018. Materials Research. 21.

[28] R. Suresh, K. Giribabu, R. Manigandan, L. Vijayalakshmi. 2014. A. Stephen and V. Narayanan, AIP Conference Proceedings. 1576, 122.